UNIVERSITY OF OKLAHOMA
GRADUATE COLLEGE

DELINEARIZATION OF POLYHEDRAL ABSTRACTIONS TO CHARACTERIZE QUANTUM ASSEMBLY

A THESIS
SUBMITTED TO THE GRADUATE FACULTY
in partial fulfillment of the requirements for the
Degree of
MASTER OF SCIENCE

By
BLAKE GERARD
Norman, Oklahoma
2021

DELINEARIZATION OF POLYHEDRAL ABSTRACTIONS TO CHARACTERIZE QUANTUM ASSEMBLY

A THESIS APPROVED FOR THE
SCHOOL OF COMPUTER SCIENCE

BY THE COMMITTEE CONSISTING OF

Dr. Martin Kong, Chair
Dr. Changwook Kim
Dr. Chongle Pan

Abstract

Increasingly complex quantum algorithms are designed in a hardware-agnostic fashion, implemented leveraging high-level programming languages, and then lowered to simpler sequences of quantum operations (gates) using a format such as the Open Quantum Assembly (OpenQASM). Unfortunately, lowering the program to a quantum assembly representation also results in a loss of structured information that can be extremely useful in later compilation passes. As a result, several quantum optimization passes simply operate on arbitrary network layers determined by the QASM-level program's dependence graph, or focus on relatively small sliding windows with peephole optimizations. For the era of Noisy Intermediate-Scale Quantum (NISQ) devices and beyond, more robust quantum compiler passes are required to tailor these decompositions and subsequent optimizations to match stringent topological and fidelity constraints.

In this paper we introduce QRANE, a tool for lifting QASM-based quantum programs into the polyhedral compilation model. QRANE groups and identifies linear relationships in the qubit indices used in two-qubit and single-qubit gates to construct iterations domains and access relations, all while preserving the original semantics of the quantum program. We explore various policies for deciding among different delinearization strategies, and discuss their effect on the quality of the reconstruction. Our experimental evaluation demonstrates the high coverage and efficiency of QRANE while also permitting to assess the potential benefits of affine transformations on large quantum circuits. Specifically, QRANE reconstructs affine iteration domains of up to 6 dimensions, and consisting of up to 128 points per domain. The parallel reconstruction of affine abstractions achieves strong scaling, facilitating the usage of higher search parameters to produce denser domains. Preliminary results also show the strong impact that affine transformations can have once domain-specific knowledge is considered.

Contents

1 Introduction

Quantum Computing (QC) has gained considerable traction in the last decade, owing to several novel high-level programming languages being introduced (QUIPPER [15], QWIRE [34], SILQ [4], Scaffold [28, 29]) as well as many efforts to improve the overall compilation pipeline in problems such as qubit allocation and layout synthesis [30, 39, 41, 53], improving the reliability of quantum programs via noise-adaptive and noise-aware schemes [33, 43, 44], and breaking abstractions [21, 37]. All of these advances have made it possible to focus on more complex application to demonstrate Quantum Supremacy [1], for instance, by focusing on the Quantum Approximate Optimization Algorithm problems [12] or leveraging domain specific framework such as OpenFermion [32].

Regardless of the programming language used to specify a quantum program, ultimately, it has to be eventually compiled down to a low-level representation such as OpenQASM [11], a quantum assembly language. At this point, the program effectively consists of long sequences of single- and two-qubit quantum gates, potentially interleaved with some simple dynamic control conditions. Lowering the representation to this level of abstraction results in significant loss of structured information that can be beneficial and heavily impactful in later compilation stages, such as qubit mapping. An example of this takes place in qubit allocation passes, where the compiler typically constructs a dependence graph from the QASM representation, proceeding to extract information from only the first few network layers, and mapping qubits that participate in long paths (or cycles) found in the dependence graph [20, 30, 39, 53]. In addition, several quantum compilation passes utilize only small sliding windows and peephole optimizations that results in finding local optima instead of global solutions. Finally, the scale of current experiments is making paramount to equally focus on scalability aspects of tools and techniques for NISQ devices and beyond [35], particularly, when quantum circuits can consist of hundreds of thousands and even millions of operations.

Recent works have proposed the use of loop-based optimization frameworks to analyze and optimize quantum programs [18, 28]. In addition, the strong impact that polyhedral compilation techniques and affine frameworks have had on high-performance computing and domain specific languages [2, 5, 6, 13, 17, 26, 45, 46, 48] leads to the next natural question: **can polyhedral and affine techniques contribute to the same extent to the field of quantum computing?**. This work is a significant step forward to answer this question. We introduce `QRANE`, a tool for automatically lifting quantum programs, written in quantum assembly, that exhibit static control (i.e. no dynamic control conditions) to the intermediate representation (IR) used in polyhedral frameworks.

`QRANE` fully automates the *delinearization* process [49], the detection and reconstruction of linear relationships among qubit indices, producing the well-known polyhedral abstractions: iteration domains (associated to what in classical computing amounts to loop iterations executed by a program statement), access relations to characterize the qubit entries used in a program, and the program schedule [14, 16]. We discuss the design and implementation of the delinearization mechanism, including the challenges faced and the meta-parameters that control the quality and behavior of the reconstruction. Our goal, is to provide the entry point by which affine analyses and transformations can contribute in the same way that they have to classical computing.

In summary, our contributions are the following: i) The design and implementation of the first quantum assembly delinearizer that produces the IR abstractions used in affine compilation frameworks (Sec. 4 and Sec. 5); ii) A comprehensive evaluation to demonstrate the quality and coverage product of the delinearization process, the efficiency of the reconstruction implementation, the effect of meta-parameters when lifting quantum assembly, and the potential impact and usefulness of polyhedral compilation techniques on circuits ranging from a few tens of operations to beyond half million gates (Sec. 6); iii) A tool serving as the entry point to exploit affine transformations in quantum compilation, and a preliminary study demonstrating the current potential.

2 Motivation and Related Work

Limitations of Current Approaches. Quantum compilers compute space-time mappings of the quantum operations (Q-OPS) in a program to a quantum processor, modeled as a (coupling) graph. Most scheduling and mapping techniques fall into one of the following categories: i) graph traversals and peephole optimizations [7, 10, 23, 27, 30, 31, 37–40, 51, 52], ii) Precise, instance-wise formulations using Integer Linear Programming and/or Satisfiability Modulo Theory solvers [3, 33, 41**?**], iii) Exhaustive enumeration and search techniques [39, 53]. The above techniques aim to tackle variations of the qubit mapping problem, which has been proved to be NP-complete [31]. Hence, scalable and yet precise methods are necessary. The three classes of techniques span the spectrum of fast but approximate results (type i), and slow (and computationally expensive) but precise solutions (types ii and iii). While some graph-based techniques performing multiple passes over the DAG could scale to millions of Q-OPS, this is not the common case. Lack of scalability hinders several of these methods, especially when they utilize *expensive* graph operations such as computing (Hamiltonian) cycles, paths with properties, and isomorphisms. Methods of the class ii, rely on precise formulations for each quantum operation of the program, and often producing $O(g^2)$

(or more) constraints on the number of Q-OPS. These techniques are only applicable to extremely small quantum programs, owing to ILP solving being double-exponential in their dimensionality.

Benefits of using QRANE. At the core, QRANE performs a grouping of quantum operations to produce more regular structures. Grouping is done by gate type and then by linear properties. This allows for the extraction of a regular, well-structured representation of the QASM program. Its benefits are two-fold: First, grouping gates that have parallel dependencies enables us to collapse these dependencies into a single structure, ultimately reducing the dimensionality of the ILP problem we solve and, consequently, its complexity (solving ILPs is double-exponential in the dimensionality). Second, a good grouping maintains scheduling freedom and flexibility by exposing a structured representation that makes the dependence patterns in the original circuit explicit. The complexity of polyhedral scheduling is (mostly) independent of the number of points in an iteration domain, as for each iteration domain exactly one shared affine scheduling function is computed

QRANE's Long Term Impact. Being the first known tool to extract a regular structure from QASM programs, we see QRANE as the foundation of a larger ecosystem of polyhedral tool-chains for QC. Analyses and optimizations over regular structures are typically both computationally cheaper and easier to understand. By exposing such regular structure, QRANE enables the development of more aggressive optimizations, e.g. scheduling in the polyhedral model or even applying machine learning over the affine IR, both of which have already brought enormous benefits in classical computing. Within the polyhedral model, lifting with QRANE already reduces the size of the program representation asymptotically. As more concrete future benefits, using our tool, the community can now focus on high-level compiler scheduling heuristics that exploit quantum domain knowledge, e.g. commutative, canceling and identity properties [37].

Computational Complexity and Scalability. One of the main motivations for this work is to demonstrate that, at the current pace, current quantum compilation techniques will hit a scalability wall. Recent qubit allocator approaches such as Zulehner et al.'s [53] and Siraichi et al.[39], which leverage A* search techniques [20] and dynamic programming, respectively, have proven that even relatively small circuits can incur high complexity execution times and memory footprints. For example, Fig.1 shows the compilation times obtained with the TKET compiler [40] on circuits of the IBM-QX circuit set [25] that have more than 100,000 gates. We can clearly notice that compilation time will continue to increase as a function of the number of QASM operations in the near term. In Section 6.3 we demonstrate that QRANE scales effectively to very large circuits.

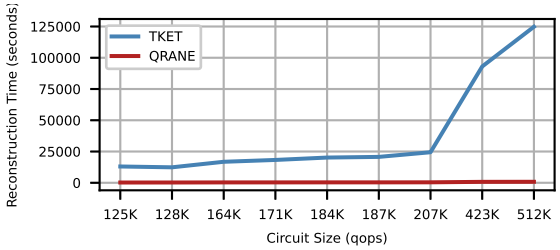

Figure 1. QRANE and TKET Processing Time for the Largest IBMQX Circuits

Impact of Re-ordering Affine Transformations. Table 1 shows an excerpt of our results that demonstrate the potential impact of affine transformations on lifted quantum assembly programs. We apply two well-known loop transformation heuristics to select circuits of the QUEKO-BIGD dataset [42] The *Improvement* column represents the circuit depth (critical path) ratio obtained directly with TKET (and without affine transformations) and while using PLuTo Min/Max-fuse. The second column shows the number of original Q-OPS in the program.

Though the applied transformations are designed for the optimization of classical computations and have yet to be tuned to the characteristics of quantum programs and devices, we nonetheless observe significant circuit depth reductions relative to circuit sizes. In particular, the transformations seem to provide greater benefits on circuits with one to two-qubit density ratios less than or equal to one, suggesting that affine abstractions can offer useful information about the temporal and spatial behavior of two-qubit gates.

QRANE lifts quantum assembly representations into an affine IR with high efficiency and efficacy, as supported by Table 2, where we present the coverage obtained for the largest circuit of the benchmark which contains 0.5M quantum operations.

QRANE achieves a compression factor of 4.2x, relative to the number of domains produced for the circuit, by aggregating quantum operations into expressive, multi-dimensional affine structures. Figure 1 and Table 2 both begin to reveal that QRANE

Table 1. Tket Final Circuit Depth with Transformed Circuits of Varying QUEKO-BIGD 20QBT Gate Densities (Ratio of single-qubit and two-qubit gates in program).

QASM	No. Input gates	TKET	PLuTo Min	PLuTo Max	Impro-vement
0D1_.8D2_1	360	524	480	504	1.09x, 1.04x
1D1_.7D2_9	405	524	381	381	1.51x
2D1_.5D2_8	405	400	348	348	1.15x
3D1_.3D2_4	405	280	240	240	1.16x
4D1_.3D2_8	495	256	176	176	1.45x
5D1_.2D2_2	540	182	160	160	1.13x

Table 2. Domain Dimensionality Profile for IBMQX's Largest (0.5M) Circuit

Dimension	Domain Count	Point Count
1D	943	959
2D	70374	185905
3D	43155	226161
4D	7943	82753
5D	896	16286
Total	123311	512064

builds an efficient and powerful IR with celerity, supporting the growing quantum compilation toolchain without becoming a bottleneck.

3 Background

In this section we briefly recap the main concepts pertaining to quantum computing, their representation and the polyhedral abstractions we attempt to reconstruct.

3.1 Quantum Computing (QC)

Quantum Bits and Gates. The basic unit of information in QC is the *qubit*. A qubit is commonly represented as a two-vector with components α and β that represent the probability that the qubit's superposition will collapse to the state $|0\rangle$ or $|1\rangle$ upon measurement, respectively. Multi-qubit states are represented as the tensor product of all constituent qubit state vectors, so the resultant state vector $|\psi\rangle$ has dimension 2^n, where n is the number of qubits.

Quantum gates, unitary operations, are modeled as $2^m x 2^m$ matrices, where m is the number of qubit the gate acts upon. While theoretical quantum gates can be designed to act on any number of qubits, in practice, all gates are decomposed into sets of "basis" gates that are physically implemented in hardware.

Quantum Circuits. Quantum circuits are a visual representation of quantum programs. Circuit diagrams model individual qubits as horizontal lanes, while gates applied to one or more qubits appear either on the affected lane or connecting two of them. Figure 2 shows a simple QASM program and its corresponding circuit representation. From here on we assume the input to `QRANE` is given in the OpenQASM format [11] format, and that its free of dynamic control dependencies.

```
qreg q[3];
t q[0];
h q[1];
s q[2];
cx q[0],q[1];
cx q[1],q[2];
```

(a) OpenQASM Code

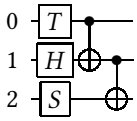

(b) Circuit Diagram

Figure 2. Simple Quantum Program with two CNOT Gates

Notably, multi-qubit gates impose *control dependencies*. Multi-qubit gates are typically extensions of single-qubit gates in that they take a *control* argument and a *target* argument. If the control qubit is in the $|1\rangle$ state, then the corresponding single-qubit gate is applied. For example, the "CNOT" gate shown in Figure 2 inverts the state of the target (bottom) qubit if the

control condition (top qubit lane) is satisfied. The SWAP gate is a unique two-qubit gate in that the qubit states are simply exchanged with no control.

3.2 Affine Abstractions

We represent quantum circuits in a polyhedral IR by encoding gate streams into the classic four structures: iteration domains, access relations, dependence relations, and schedules. **Iteration Domains** are sets in $\mathbb{Z}^n$ whose points represent the dynamic instances of multi-dimensional loops, where the loop bounds are affine functions of outer loop iterators and symbolic (constant) parameters. In the case of quantum gate streams, we assume an underlying stream generator takes an affine loop nest form, wherein quantum register accesses are affine functions of the loop iteration variables. Thus, we can group together multiple OpenQASM operations whose corresponding register accesses appear to be governed by the same affine functions. **Access Relations** are functions of the iteration domain, $F^S : \mathbb{Z}^d \mapsto \mathbb{N}$, that model indices accessed on quantum registers. Since control qubits are unaltered by multi-qubit gates and target qubits can undergo state change, we define *read* relations and *write* relations as a mapping of iteration domain points to control and target qubit accesses, respectively. **Dependence Relations** represent ordering constraints among instances of iteration domains. Just as in the classical case, quantum programs exhibit flow, anti, read, and write dependencies based on control and target qubit accesses. As we show in 5.6, after encapsulating gate operations into affine iteration domains, we can convert time-space (global operation number) instance-wise dependencies imposed in the original gate ordering to the domain-space, allowing the description of coarse-grained dependence relations via affine functions. **Schedules** are affine relations that assign logical multi-dimensional time-stamps to iteration domain points. Our work uses a single 1-dimensional linear schedule preceded by a single scalar dimension encoding the chunk identifier when performing parallel lifting.

4 Overview

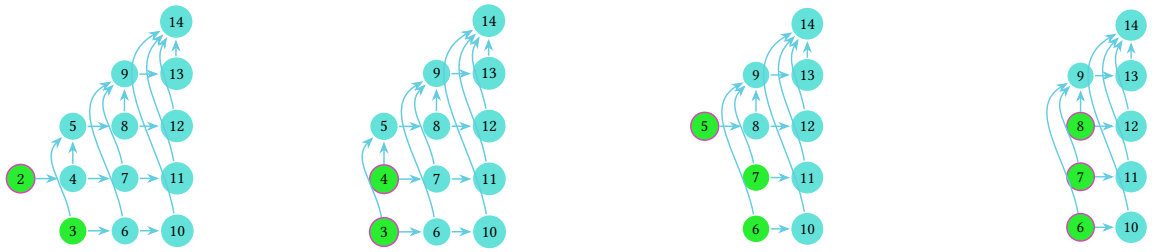

(a) Time-step 3 **(b)** Time-step 4 **(c)** Time-step 5 **(d)** Time-step 6

Figure 3. Evolution of 1D Reconstruction. Green represents Frontier, Red represents selected Domain.

We first provide an overview of our approach to the delinearization of quantum gate streams. The Quantum Fourier Transform (QFT) circuit on five qubits [8], shown in Figure 4, serves as our motivating example. Walking through each step of QRANE's reconstruction process, we outline the techniques used in the one-dimensional and N-dimensional reconstruction phases, describe the formation of access relations, and discuss potential scheduling options.

4.1 1D Domains and Access Relations

The first step is to generate one-dimensional iteration domains. That is, QRANE will first look for gate sequences whose qubit register accesses *could* have been generated by a single affine loop. The immediate observation and convenient constraint is that the number of points in any one-dimensional iteration domain must be less than or equal to the size of the qubit register. Thus, QRANE (mostly) limits its view of the circuit to the set of gates that most recently accessed each qubit in the register (a reconstruction improving heuristic that does take a look deeper into the circuit is discussed in Section 5.2). We refer to this set of gates as the circuit "frontier", which is equivalent to the set of vertices in the time-space dependence graph of in-degree zero. At each time-step in the one-dimensional reconstruction phase, QRANE examines the frontier of the circuit and attempts to find an affine function that generates the largest gate access sequence possible. The gates covered by the chosen function are then removed from the circuit, allowing their immediate successor gates to enter the frontier. This process is repeated until the circuit is empty. We note that in this context, an iteration domain contains points of only one gate type, so the analysis is performed for the gate type that most frequently occurs in the frontier, so as to maximize the chance of constructing a large iteration domain at each time-step.

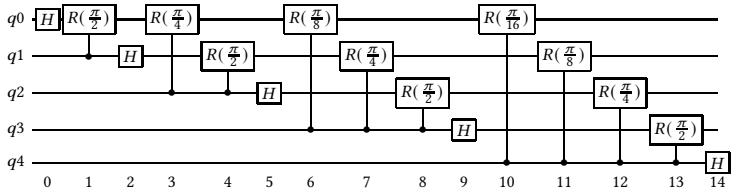

Figure 4. Quantum Fourier Transform (QFT) on Five Qubits

Figure 3 shows the evolution of the 1D reconstruction over the dependence graph of QFT-5. The first and second time-steps are elided, because the dependence frontier is occupied by only gate one in time-step one, and by only gate two in time-step two. QRANE considers these points as "stray points" as they don't follow the greater dependence pattern evident in the circuit; singleton domains are created to house these points, and they are then removed from the dependence graph. The vertices representing gates two and three enter the frontier in time-step 3. Since domains may only cover one gate type, a decision must be made to draw a domain from gate two or three. QRANE engages in a breadth-first lookahead here, computing the ratio of one to two-qubit gates immediately neighboring the vertices of the frontier. Finding the ratio to be one, QRANE defaults to build a domain for one-qubit gates, putting gate two in a singleton domain.

```
       Domains                  Read/Write Relations
# Structures repeat with unique X identifier for H gates
SX[i] : 0 <= i <= 0;      SX[i] -> q[i];

# Structures representing each grouping of R gates.
 S1[i] : 0 <= i <= 0;      S1[i] -> q[i+1], q[i]
 S3[i] : 0 <= i <= 1;      S3[i] -> q[i+2], q[i]
 S6[i] : 0 <= i <= 2;      S6[i] -> q[i+3], q[i]
S10[i] : 0 <= i <= 3;     S10[i] -> q[i+4], q[i]
```

Figure 5. 1D Iteration Domains and Access Relations

```
          Extended Structures
# All H gates aggregated into one domain
S0[j, i] : 0 <= j <= 4 and i = 0;
S0[j, i] -> q[j];

# All R gates aggregates into one domain
S1[j, i] : 0 <= j <= 3 and 0 <= i <= j;
S1[j, i] -> q[j+1], q[0*j+i];
```

Figure 6. 2D Iteration Domains and Access Relations

From here on out, QRANE exploits a consistent pattern where the frontier is occupied by a single H gate and a number of controlled phase gates. In time-step 4, we have R_3 and R_4 now in the frontier, giving QRANE the opportunity to test for linearity amongst both qubit access arguments of the two gates. For two-qubit gates, QRANE considers the control and target qubits to serve as coordinates in a 2D coordinate space, immediately revealing linearity between these points (of course, any affine line will suffice). QRANE records the qubit argument strides, and ensures a consistent lexicographic ordering between all points in the domain. The read/write access relations $[i] \rightarrow q[2]$, $q[i]$ are constructed based on the positive stride of 1 for the target qubit accesses. Furthermore, lexicographic consistency is needed to ensure that the gate access sequence can be feasibly modeled with an affine multi-dimensional schedule. The constraints placed on 1D domain creation are discussed further in Section 5.2.

The above pattern is repeated until the dependence graph is empty, yielding the iteration domains and access relations shown in Figure 5.

4.2 Raising Dimensionality through Merging

We can increase the dimensionality and improve the efficiency of our affine abstractions by repeatedly "merging" lower-dimensional structures into single structures that characterize N-D loop nests. A merger of two domains requires that we introduce a new linear dimension into the structure that serves as the "outer-most" loop variable, while the existing dimensions of the constituent domains are preserved as the "inner-most" loop variables. This step allows QRANE to represent sequences of *d*-dimensional domains as a single linearly consistent system of *d+1* dimensions.

Continuing with our example of Fig. 4, QRANE recognizes that the 4 *R* gate sequences can be reproduced by a system of 2 linear variables, *j* and *i*, where *j* controls the number of R gate sequences, and *i* controls the number of *R* gates occurring in each sequence. We can also reproduce the qubit access sequences by varying the control accesses by a linear function of *j* and the target accesses by a linear function of *i*. QRANE also recognizes that, by fixing the variable *i* (distinct from that of the R gate system) to a single iteration and bounding *j* to reflect the five singleton *H* gate domains. The extra linear variable in this system is a byproduct of the dependence graph-based reconstruction, but the compression effect is identical to that of a single domain on one variable. At this point no further merges are possible, so QRANE completes the reconstruction phase. The resulting N-Dimensional affine abstractions are depicted in Figure 6.

QRANE searches for combinations of domains to merge together, up to a user-defined limit, permitting a merger only if the candidates meet the conditions discussed in Section 5.5. Once the list of candidate domains is produced, QRANE iteratively selects and removes the largest candidate domains by cardinality, until the set is empty. This process continues to N-dimensions until no further changes are possible, as is the case in our example after reaching the 2D structures shown in Fig. 6.

4.3 Scheduling

The schedule maps the points of each iteration domain to some multi-dimensional time coordinate composed of both scalar and linear dimensions. For example, the hand-written schedule in Figure 7 exactly reproduces the original circuit by mapping the *j*'th iterations of domain S0 to an even outer time dimension and those of S1 to an odd outer time dimension. The *i* component of the schedule produces the inner-most loop at each outer time dimension.

By default, QRANE constructs the *implicit* schedule for the program, which simply maps the points of each iteration domain to the original 1D time-space of the program. However, QRANE may invoke the scheduling capabilities of ISL to produce legal transformations that re-order the quantum operations to achieve some optimization goal. For example, QRANE can leverage the *minfuse* and *maxfuse* heuristics of the PLuTo scheduling algorithm in attempt to minimally or maximally fuse the loops encoded in our affine abstractions. The re-ordering produced with the *maxfuse* option is shown Figure 7. This schedule interleaves the points of each domain to minimize all dependence distances in the time-space. The effect of these schedule transformations on circuit compilation metrics is investigated in Section 6.

```
                  Implicit Schedule
S0[0, 0] -> [0]; S0[1, 0] -> [5];
S0[2, 0] -> [9]; S0[3, 0] -> [12]; S0[4, 0] -> [14];
S1[j, 0] -> [1+j] : 0 <= i0 <= 3;
S1[j, 1] -> [5+j] : 0 < i0 <= 3;
S1[j, 2] -> [8+j] : 2 <= i0 <= 3; S1[3, 3] -> [13];

             PLuTo Maxfuse Schedule
S0[j, 0] -> [j, j, 0] : 0 <= j <= 4;
S1[j, i] -> [j, i, 1] : j <= 3 and 0 <= i <= j;
```

Figure 7. Schedule Examples for QFT-5

5 Recovering

We now present our methodology for reconstructing iteration domains, access relations, and the identity schedule for a given OpenQASM file. The lifting is divided into 3 stages: dependence analysis, 1D and N-D domain recovery. Firstly, since we deal with straight-line code, we assign each quantum operation (Q-OP) a *global id* corresponding to its sequence number in the program. We refer to this bijection of $\{global\,id \rightarrow \text{Q-OP}\}$ as the *time space* of the original program. Furthermore, we maintain a separate bijection of $\{global\,id \rightarrow domain\,instance\}$, hereafter called the *domain space*, so that each Q-OP in the program is associated with a specific point in some iteration domain. The range of the relation is initially empty and is continuously updated throughout the reconstruction process to reflect set membership of reconstructed iteration domains.

Our reconstruction requires all gates on 3 or more qubits to have been previously decomposed into equivalent one and two-qubit gates. In addition, we defer to future work the handling of dynamic control dependences.

5.1 Auxiliary Dependence Analysis

We first perform a quick dependence analysis pass on the OpenQASM stream. As in [22], the DAG creation process from a qubit access trace is straightforward. We annotate each qubit with the global id of the gate that most recently wrote to it, and draw dependencies between all subsequent gates reading from and writing to that qubit. The annotation is then updated to reflect the latest write. The result is a set of point-to-point dependencies in the original time space of the input sequence. This simplified dependence representation is necessary for the subsequent components of QRANE.

5.2 One-Dimensional Domain Recovery

Many prior works in trace analysis individually process memory access streams of each unique instruction, attempting to find minimal affine loop nests capable of reconstructing the access patterns. In the context of OpenQASM programs, we have very little auxiliary information to differentiate sets of quantum operations as belonging to the same or separate generating instructions. Thus, we can set rules for operation grouping that provide precise and correctness-preserving limitations on the reconstruction.

Firstly, we require our future assembly-generating-statements to issue accesses of a single gate type. Secondly, as described in Sec. 4.1, QRANE asserts linear relationships among quantum gates based on their qubit access patterns. In the 1D recovery stage then, QRANE attempts to draw these relations between the set of gates that have most recently accessed each element of the qubit register. This set of gates is equivalent to the "frontier" of the dependence graph, or those vertices that have zero in-degree. QRANE iteratively fetches the frontier of the dependence graph, finds the affine function of one variable that covers the largest number of points in the current time-step, and removes the covered gates off the dependence graph while updating the *domain space* to reflect the new gate grouping. The removal operation cause an in-degree reduction for all neighbors of the covered set, of which some will enter the frontier. Alg. 1 performs these steps.

Algorithm 1: Construct One-Dimensional Domains

Input: G: Data Dependence Graph
Output: D: Mapping of unique ID to iteration domain

```
1  Let domain_count = 0
2  Let d = 1
3  while G not empty do
4      F = copy_frontier (G)
5      Q1, Q2 = separate_by_num_args (F)
6      DOM = selection_policy (G, d, Q1, Q2)
7      G.remove (DOM.points)
8      D[domain_count] = DOM
9      domain_count += 1
10 return D
```

Once the dependence frontier is retrieved, we split the nodes into sets of one (*Q1*) and two (*Q2*) qubit gate operations per our single gate type criterion. While these sets are further subdivided by gate type, only the most frequently occurring gate type is chosen to comprise *Q1* and *Q2*. One critical decision that QRANE must make here is, in the current-time step, from which of these sets should a domain be constructed? While decisions are correct with only a view of the frontier, QRANE may optionally perform a lookahead in the dependence graph up to breadth d (default two), computing the ratio r of one to two qubit gates among the immediate d neighbors of each vertex in the frontier. The rationale of this heuristic *selection policy* is that QRANE ought to select *Q1* if $r < 1$ because more 2-qubit gates are expected to enter the frontier in future-time steps, exposing more 2-qubit gates for analysis in a single time-step, and vice versa for the selection of *Q2*. The other cases for r are shown in Alg. 2. The core process of finding the most profitable affine function is the same regardless of the selection, though one added filtering step for 2-qubit gates is discussed in 5.3.

Algorithm 2: One Qubit or Two Qubit Selection Policy

Input: G: Data Dependence Graph, d: Lookahead depth,
$Q1$, $Q2$: One and two qubit vertices ∈ G.frontier, respectively
Output: Q: Chosen Gate Type

```
1  Let forecast.ones = 0, forecast.twos = 0
2  foreach vertex v ∈ Q1 do
3  |   N = get_neighbors_by_depth (G, v, d)
4  |   foreach neighbor n ∈ N do
5  |   |   forecast.increment_counter (n.num_arguments)
6  // repeat 2-5 for Q2
7  if forecast.ones = |G.frontier|: return Q1
8  if forecast.twos = |G.frontier|: return Q2
9  if forecast.twos >= forecast.ones: return Q1
10 return Q2
```

5.3 Finding Affine Qubit Access Functions

Given a set of qubit access arguments Q drawn from the gate set chosen by the selection policy, we construct a directed graph G where:

$$\text{Vertices } V = Q, \text{ and Edge } e = \{q_1, q_2\} \in G \text{ iff } q_2 > q_1,$$
$$\text{and Annotation } a = (\alpha, \beta) \text{ on } e \text{ where}$$
$$\alpha = q_2 - q_1 \text{ and } \beta = lexicographic\_order(q_1, q_2) \quad (1)$$

where $lexicographic\_order(q_1, q_2)$ represents the third restriction on the reconstruction. The function determines whether q_1 and q_2 are lexicographically positive or negative in the program time-space. Qubit access sequences must be both produced by some affine function, *and* maintain a consistent lexicographic ordering, lest a valid affine schedule for the sequences be impossible.

Each annotation carries the stride between two points, as well as their lexicographic ordering. We perform a depth-first search on each vertex in the topological ordering of G, shown in lines six and seven of Algorithm 3, establishing a baseline annotation on the first edge of each path and only extending a path when the annotations are equal to the baseline. The stride of the longest, constant annotation path found in that search is selected as the stride of the affine function covering the chosen domain from the frontier. The lexicographic ordering must also remain constant between points because a domain whose constituent points have both positive and negative lexicographic ordering cannot be produced by an affine schedule.

In the case of two qubit gates, we first find the largest co-linear subset from the *Q2* set by considering the control and target qubits as coordinates in a 2D space in order to reveal point groupings that could potentially exhibit linearity. We iteratively perform the aforementioned search procedure to ensure constant stride and lexicographic continuity amongst the largest set of co-linear points.

Algorithm 3: One-Dimensional Domain Selection

Input: Q: Set of points from *G.frontier*
Output: Selected Domain

```
1  Let Q' = ∅ if Q.is_two_qubit_gate_set then
2  |   Q' = largest_colinear_subset (Q)
3  else
4  |   Q' = Q
5  Let P = ∅
6  foreach vertex v ∈ topological_ordering (G) do
7  |   Perform Depth-First Search with source v, recording annotation a' of each outgoing edge, and recursing on paths with
   |     annotations equal to a'
8  |   Store longest such path in P
9  return construct_domain (max ((P)))
```

5.4 Access Relations

A key product of the one-dimensional reconstruction phase is an "access matrix" that simply encodes all of the register accesses made by a domain. Its form is shown in the matrix below: 2.

$$\begin{bmatrix} i_{1,1} & \dots & i_{1,m} & 1 & a_{1,1} & 1 & a_{1,2} \\ \vdots & \ddots & \vdots & \vdots & \vdots & \vdots & \vdots \\ i_{n,1} & \dots & i_{n,m} & 1 & a_{n,1} & 1 & a_{n,2} \end{bmatrix} \tag{2}$$

This matrix encodes a system of n quantum operations whose register arguments *could* be generated by affine function of m variables. Thus, each point in the potential new domain occupies one row of the matrix, and the values in the first m columns of each row represent the integer values of each loop iteration variables corresponding to that point in the domain. The two fixed column vectors of constant value one represent the constant term of the affine function potentially generating the access sequence. The columns $a_{n_i,1}$ and $a_{n_i,2}$ take the value of the control and target qubits for each operation, respectively. The matrix in Equation 2 thus models a two-qubit gate system, and a domain of one-qubit gates would have just one constant column and one arguments column. The solution to this system of equations then gives affine access relations for each point in the domain, allowing us to generate *Read* and *Write*-relations mapping each point in a domain to a multi-dimensional affine access to the qubit register. However, the unsolved state of this matrix is retained and heavily utilized in the N-Dimensional recovery phase — discussed in 5.5 — where the concatenation and extension of access matrices for multiple domains is solved and tested for consistency before admitting a merger of those domains.

5.5 N-Dimensional Domain Reconstruction

Once all gate accesses are characterized by one-dimensional affine abstractions, QRANE iteratively merges lower-dimensional domains into higher-dimensional domains by augmenting structures with new iteration variables, as per Alg.4. QRANE will examine a set of d-dimensional domains in effort to detect repeated or similar register access patterns by equivalent gate types. If the access patterns made by multiple domains can be generated by a consistent *(d+1)*-dimensional affine loop nest, QRANE will "merge" the domains into a single *(d+1)*-dimensional domain that forms some polyhedral structure in that space. This step is necessary to improve the expressiveness and efficiency of our abstractions, enhancing the quality of information available when computing schedule transformations.

We first describe the conditions that must be met for two d-dimensional domains, A and B, to be merged into a single higher-dimensional domain. These are higher-dimensional generalizations of the rules described in Sections 5.2 and 5.3:

***A* and *B* have equivalent gate types.** This is a requirement to maintain the gate type consistency stipulation from Section 5.2

***A* and *B* are lexicographically consistent.** Just as the points of any one-dimensional must be lexicographically consistent relative to one another, the lexicographic ordering of the domains must match the original lexicographic ordering of the lower-dimensional domains. That is, if A and B are lexicographically positive themselves, then all points in B must be greater than all points of A in the time space. Thus, A and B must be disjoint in the original time-space of the program to ensure schedule-ability of their higher-dimensional extended domain in an affine multi-dimensional space.

***A* and *B* form a consistent system of *(d+1)* dimensions.** It may not be possible to form a consistent linear system on *(d+1)* variables that governs the combined qubit access patterns of A and B. To test for consistency, we build the new access matrix C of *(d+1)* dimensions via *concatenation and extension*:

$$A = \begin{bmatrix} 0 & 1 & 0 \\ 1 & 1 & 2 \end{bmatrix} \quad B = \begin{bmatrix} 0 & 1 & 1 \\ 1 & 1 & 3 \end{bmatrix} \quad C = \begin{bmatrix} 0 & 0 & 1 & 0 \\ 0 & 1 & 1 & 2 \\ 1 & 0 & 1 & 1 \\ 1 & 1 & 1 & 3 \end{bmatrix}$$

The prepended column represents the *(d+1)*'th linear variable. This new access matrix is then reduced to test for consistency.

QRANE searches the set of lower-dimensional domains, admitting any groupings of domains that meet the three previously described qualifications as *candidate* higher-dimensional domains. Since some OpenQASM circuits may be large and highly irregular, a large number of lower-dimensional domains may be produced; QRANE performs the candidate search up to a user-defined *search limit*, offering the user a trade-off between execution time and the quality of the reconstruction.

QRANE selects domains from this list to proceed to the next iteration of the reconstruction. While the candidate list is not empty, QRANE picks the largest domain by cardinality from the list and removes all other domains that reference the now covered set of lower-dimensional domains. At the end of this process, QRANE has a set D of d-dimensional domains that were not merged with any other domains, and a set D' of selected *(d+1)* -dimensional domains. D is offloaded to a set of *unchanged domains*, and D' becomes the focus of the search for the next iteration of the N-Dimensional reconstruction process. The process completes when QRANE makes no further mergers at a given level.

Algorithm 4: Construct n-Dimensional Domains

Input: D: 1D iteration domains, l: Search Limit
Output: D': ND iteration domains

```
Let D' =
while D not empty do
    Let W =
    C = {D × D where D_i D_j is linearly consistent and j − i >= l}
    while C not empty do
        d = max_cardinality (C)
        W.insert (d)
        C.erase (x_i ∈ d)
    D' = D - W
    D = W
return D'
```

5.6 Scheduling

As identity schedule, QRANE utilizes the implicit 1D linear schedule representing the operation number of a given iteration domain point. We thus defer the task of computing a more compact schedule to ISL. This doesn't pose any scalability issue, specially when leveraging our parallel reconstruction feature. All affine transformations available in ISL can then be used, in particular the Pluto minfuse (nofuse) and maxfuse loop fusion heuristics [5, 47], which we evaluate in Sec.6.

5.7 Parallel Lifting

QRANE leverages the *implicit* one-dimensional linear schedule (i.e. operation number) to enable the parallel reconstruction of the affine IR. This is achieved by decomposing the input QASM into N disjoint chunks, each of which can be lifted in parallel. Optionally, the user may insert OpenQASM "barrier" statements into circuit, forcing QRANE to independently delinearize and schedule the sub-circuits delineated by the barriers. While this has the obvious advantage of accelerating the reconstruction process, it also has the (unforeseen) benefit of allowing us to use larger values for our search parameters, thereby improving QRANE's reconstruction quality. In addition, we introduce in the implicit schedule a leading scalar dimension representing the chunk number, converting it to a schedule with two time-components. Such an additional schedule dimension yields semantically equivalent results when passed to ISL's dependence analysis, but the structural representation of these dependences might be different and has the potential to impact later scheduling decisions, e.g., by splitting the index space into multiple pieces a scheduler can assign independent linear schedules for each piece. A comparison of the *parallel vs. sequential reconstruction* is included in the Appendix, while results presented in Sec. 6 focus exclusively on the parallel lifting.

5.8 Verification

The user may request that QRANE run its verification passes to ensure correctness of the reconstruction and scheduling. QRANE invokes ISL's code generation utilities to produce C code capable of generating OpenQASM from its affine abstractions. The resulting OpenQASM stream is sent through QRANE's dependence analysis in order to verify the results.

QRANE performs four checks of increasing complexity. First, QRANE checks that all Q-OPS are accounted for in the affine abstractions by invoking the Barvinok Integer Set Counting library [**?**] to count the points of the iteration domain produced for the second. Next, QRANE checks for lexicographic positivity in the minimum delta of the reordered and original dependences. A lexicographically negative delta implies that one or more original dependences have been violated in the reordered OpenQASM. Next, QRANE tallies up the number of accesses to each qubit by each gate type in the original program, and checks that the same tallies of the reordered program are exact, ensuring that no operations were left out of the reconstruction and all access relations are correct. Finally, QRANE utilizes the NetworkX [19] implementation of the VF2 [9] algorithm to check for semantic isomorphism between the reordered and original dependence graphs. That is, each vertex in the dependence graph is labeled with the full quantum operation it represents, and the isomorphism check only admits a vertex mapping if their labels are identical. These four verification steps show the user the correctness of QRANE's reconstruction, most importantly that any re-ordering of the OpenQASM code has not violated any dependences.

6 Evaluation

In this section, we apply QRANE to three large OpenQASM benchmark sets to evaluate the effectiveness of the reconstruction and the optimization potential provided by the recovered affine abstractions. Section 6.2 examines the reconstruction quality in terms of recovered domain dimensionality and density. Section 6.3 examines QRANE's scalability. Finally, Section 6.4 explores the impact of two affine schedule transformations on circuit compilation metrics.

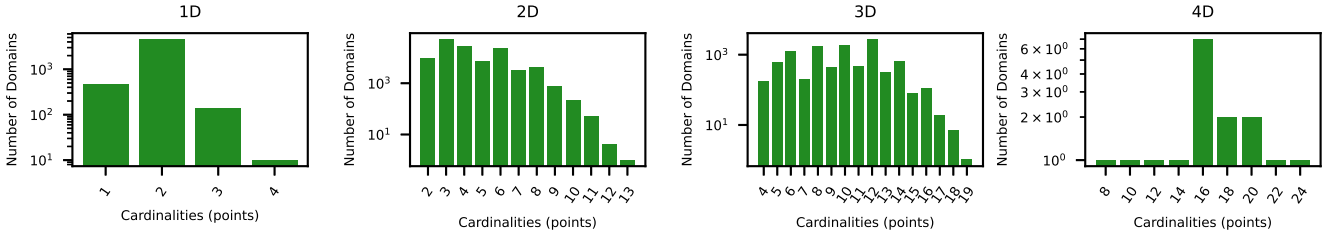

Figure 8. Reconstruction Quality for QUEKO-BSS-20QBT

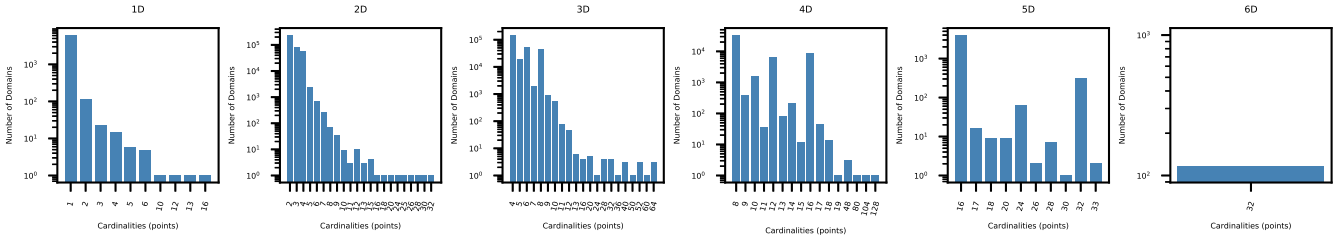

Figure 9. Reconstruction Quality for IBMQX

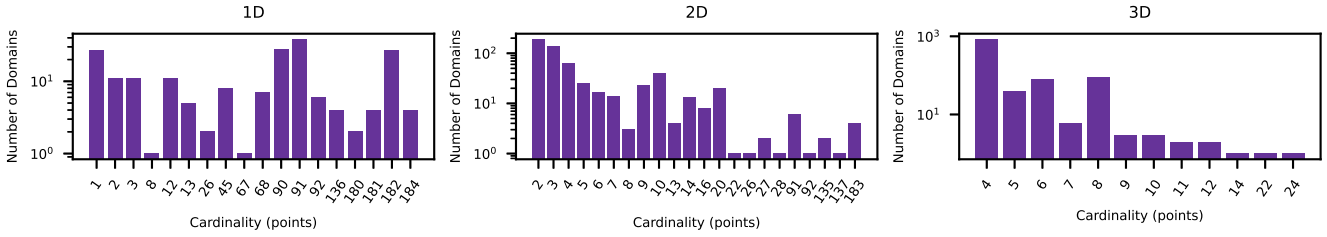

Figure 10. Reconstruction Quality for QASMBench-Large

6.1 Experimental Testbed

We evaluate QRANE on three benchmark sets, **QUEKO** by Tan and Cong [42], IBMQX [25], a large resource of quantum circuits gathered by Zulehner et al. from RevLib [36, 50] and prior works, and **QASMBench** by Li et al. [**?**] at Pacific Northwest National Lab.

QUEKO is a set of quantum circuits designed by construction with known optimal depth. We use two circuit sub-classes of **QUEKO**, the **BIGD** set and the **BSS** set. The former consists of small circuits with varying gate densities (proportions of 1-qubit and 2-qubit gates), while the latter was designed for *scaling studies*, with ten sub-classes of circuits with optimal depth values and ten variations within each class.

IBMQX [53] consists of 158 circuits pre-mapped to legacy IBMQX architectures using between 5 and 16 qubits. These circuits vary dramatically in gate counts, ranging from five to half a million gates. Since these circuits were targeted for smaller architectures and all follow a similar mapped structure, the circuits tend to be very narrow.

QASMBench provides several low-level implementations of quantum algorithms and subroutines at the core of chemistry, optimization, machine learning, and more. Across the small, medium, and large categories, the circuits exhibit a variety of widths (qubits), depths, gate densities, and other useful metrics. We chose to focus on the set of large circuits for this evaluation,

as our results for the small and medium classes were very similar to those of the IBMQX benchmarks; large circuits reveal interesting qualities of QRANE's behavior with respect to the relationship between circuit width, depth, and gate density. All QASMBench circuits were decomposed several times in QISKIT such that all gates were one and two-qubit decompositions and all gate blocks were inlined.

We utilize Tket version 0.13 to collect compilation metrics. We use Barvinok library version 0.41.4 and ISL 0.23 for operations on integer sets and maps, as well as for the latter's scheduling capabilities. All experiments were run on an AMD Ryzen Threadripper 3970x 32-Core CPU operating at 4.5GHz. and equipped with 128 GB RAM.

6.2 Reconstruction Coverage

To assess the quality of QRANE's reconstruction, we focus on the QUEKO-BSS and IBMQX benchmarks because their larger circuits pose a greater compression challenge. Figures 8 and 9 chart the "Reconstruction Profile" obtained with with a search limit of 1024 and lookahead-breadth of two. The Reconstruction Profile contains, for all domain dimensions produced for a benchmark, all of the domain cardinalities recovered for those dimensions and the number of domains of those cardinalities. QRANE's primary goal is to compress as many Q-OPS into high density iteration domains as possible, relying on dimensionality extension to pack more points into a single domain while respecting the linearity of the system. While QRANE has to shuttle many "stray points" into domains of 1, 2, and 3 points, in QUEKO-BSS, domains of cardinality four and above contain 2.59x as many points as contained in lower cardinality domains. QRANE performs even better on the IBMQX benchmark, assigning 2.99x times as many points into domains of cardinality four or higher than of lower-cardinality domains.

QRANE produces very dense lower-dimensional domains for the QASMBench-Large circuits. Most circuits involve anywhere form 16-27 qubits, along with the "ising_model" outliers on 500 and 1000 qubits. QRANE greatly benefits from a wider qubit register, since the density of one-dimensional abstractions is directly limited by the size of the register. If QRANE can shuttle more points into dense 1D domains, then it will have less work to do in merging irregular, heterogenous domains produced over smaller registers, such as in IBMQX. Furthermore, QRANE prefers low depth, high qubit occupancy (gate density) circuits. Such circuits exhibit patterns where one and two-qubit gates are applied in parallel across the entire register, leading to fewer long gate paths in the dependence graph. The ising_model circuits are the perfect use cases for QRANE; these circuits have very wide registers, and are amongst the lowest depth and highest gate density circuits in the benchmark set.

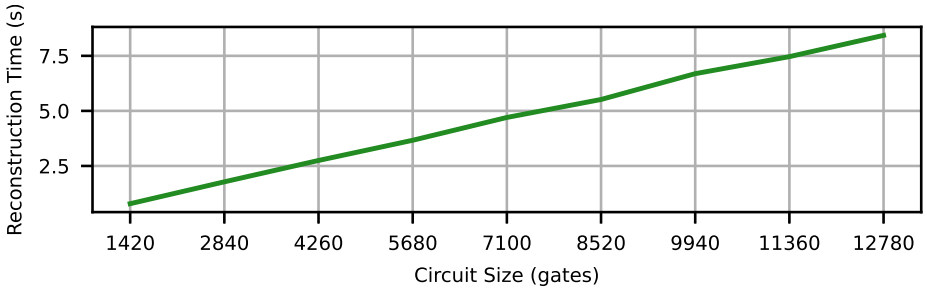

(a) QUEKO-BSS-20QBT

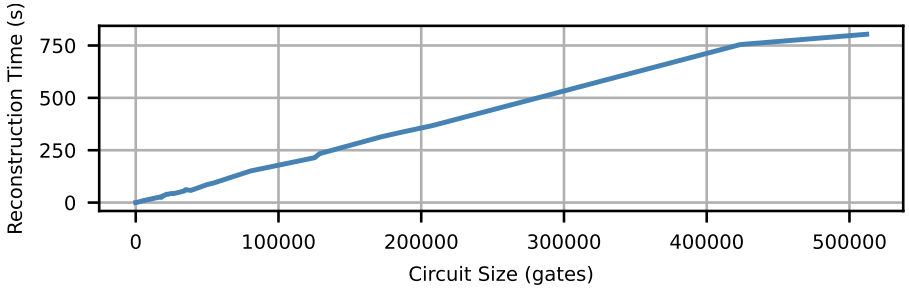

(b) IBMQX

Figure 11. Sequential Subcircuit Reconstruction Scaling Time vs Circuit Size for QUEKO-BSS-20QBT and IBMQX

6.3 Reconstruction Scaling

We briefly examine the scalability of QRANE's reconstruction. Figures 11a and 11b show average reconstruction time over increasing circuit sizes. For QUEKO-BSS, we chunk all files into sub-circuits of 1000 operations, and impose no N-Dimensional search limit within each sub-circuit. For IBMQX, we also chunk all files into 1000 gate sub-circuits, but also impose a search limit of 512 domains. We do not here that, while the circuits are divided into sub-circuits, the execution time is indicative of *independent, sequential processing* of each sub-circuit. This was done to highlight the noticeable scalability benefits of decomposing the circuit into sub-circuits and performing independent reconstructions, all without sacrificing reconstruction quality. The addition of multi-threading directives, then, gives even faster results. These plots show that QRANE scales uniformly with increasing circuit size, which allows QRANE to be a part of a larger compilation toolchain without becoming a bottleneck. Furthermore, custom gate subroutines (marked by the "gate" signifier in OpenQASM 2.0) can be delinearized just once, and the recovered abstractions simply reused for each occurrence of that subroutine in the circuit, further reducing reconstruction time. A further look into QRANE's scalability is provided in the Appendix.

6.4 Exploring Affine Transformations

In this section, we evaluate the effect of two polyhedral schedule transformations methods — PLuTo Minfuse and PLuTo Maxfuse — on the Gate Count and Circuit Depth metrics after optimization and routing in Tket. Metrics are collected for architectures IBM Montreal (27 qubits) and IBM Brooklyn (65 qubits) [24]. Here we have chosen the QUEKO-BIGD set to examine the effect of these transformations on circuits with a variety of one and two-qubit gate densities (ratio of number of single-qubit gates to two-qubit gates). **We remind the reader that these heuristics are from classical computing**, and model classic data locality. Hence, results from Table 3 should be interpreted as an exploratory study of the two ends of the loop distribution/fusion spectrum. **The design of new scheduling heuristics with objectives leveraging quantum domain knowledge, similar in spirit to Shi et al's work [37], is left as future work enabled by QRANE**.

Rescheduled (and semantically equivalent) QASM programs are obtained from building and executing the loop structure defined by a given affine transformation. Original and re-ordered circuits are then provided to TKET for compilation, and absolute gate count and circuit depth are collected. TKET has been configured to run NoiseAwarePlacement, FullPeephole Optimization, Routing, and Rebase to IBM gates [40].

We show in Table 3 the *baseline* metric (gate count and circuit depth) obtained on each architecture. We split the circuits into instances exhibiting improvement and deterioration. These are represented as *negative* (correspondingly, positive) variations over the baseline. One can observe then, overall, deterioration can range from 22% to 28% on both metrics, while improvement can range from 12% to 19%.

Figure 12 shows the absolute Gate Count and Circuit Depth metrics collected with TKET. For each gate density vector in the QUEKO-BIGD benchmark, we provide the original OpenQASM file as well as the re-ordered OpenQASM generated by the affine Minfuse and Maxfuse transformations. The data shows that for both Gate Count and Circuit Depth metrics, the gap between the baseline and transformations tends to narrow as the density of two-qubit gates increases. In these cases, we suspect that as more two-qubit gates are introduced, there is a greater opportunity for re-ordering operations to expose optimize-able patterns to local circuit re-writing routines. We intend to explore more precise re-ordering techniques in future work.

We observe that the worst deterioration takes place when the density of 1-qubit gates (d1) is greater than that of 2-qubit gates (d2). This is expected since 2-qubit gates tend to dominate the qubit mapping process due to them being the root cause for the insertion of SWAP operations. We observe that the Maxfuse heuristic tends to outperform the Minfuse heuristic at low one-qubit gate densities, while this gap closes to minimal or no performance difference as one-qubit gate density increases.

We emphasize again that the Minfuse and Maxfuse heuristics are designed for classical program optimizations, and as such, are fairly agnostic to the quantum context in which we are working. These heuristics do not take into account the device architecture or hardware fidelity metrics, nor are they tuned to the common behaviors and structures of modern quantum programs. We suspect that in cases of improvement, the transformations were able to better reveal to the optimizer candidate patterns for replacement, while in cases of deterioration, these patterns were inadvertently made harder to detect [**?**]. Nevertheless, we believe that future affine transformations utilizing QRANE as a starting point will be able to better expose better expose commutivity relationships and connectivity patterns among dense two-qubit gate routines. **The close gap in Tket's average metric performance between the original circuits and the re-ordered circuits, in spite of the generalized nature of the applied heuristics, foretells the potential for strong quantum-contextualized polyhedral transformations enabled by QRANE**.

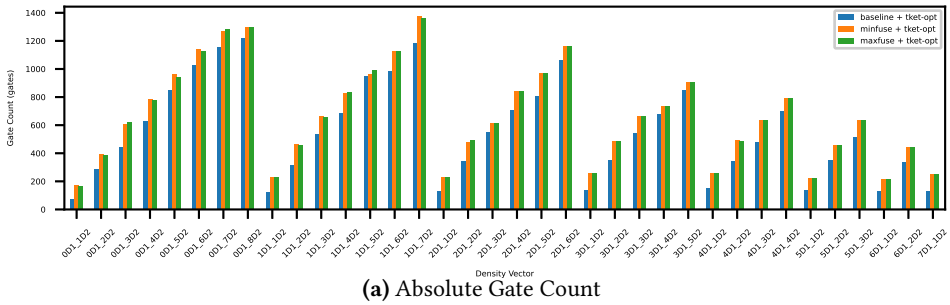

(a) Absolute Gate Count

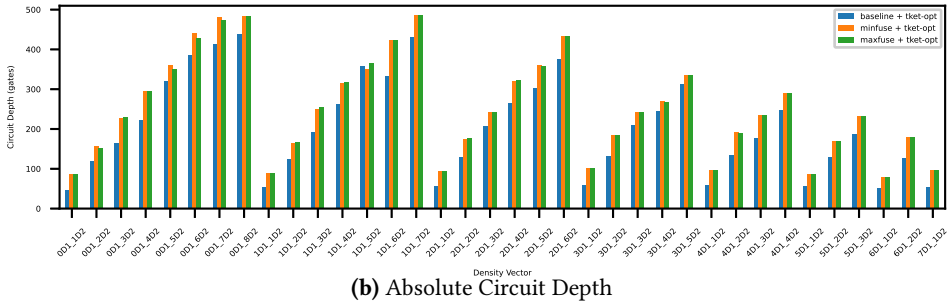

(b) Absolute Circuit Depth

Figure 12. Impact of Transformations on QUEKO-BIGD with Tket for IBM Brooklyn

Table 3. Mean Improvement/Deterioration of Affine Transformations on Gate Count and Circuit Depth - QUEKO BIGD.

Result	**TKET**	**Improvement**		**Deterioration**	
Transformation	**Gate Count (gates)**				
	baseline	minfuse	maxfuse	minfuse	maxfuse
Montreal	516.32	-98.13 (40)	-88.75 (44)	117.78 (296)	118.81 (292)
Brooklyn	553.44	-74.92 (36)	-67.59 (39)	137.36 (300)	138.20 (297)
Transformation	**Circuit Depth (gates)**				
	baseline	minfuse	maxfuse	minfuse	maxfuse
Montreal	193.25	-30.12 (51)	-28.34 (50)	49.94 (285)	49.01 (286)
Brooklyn	204.93	-36.02 (45)	-33.52 (46)	58.67 (291)	58.10 (290)

7 Conclusion

In this paper we have presented the design and implementation of QRANE, the first polyhedral reconstruction tool that lifts quantum assembly into an affine IR. QRANE performs the delinearization of qubit indices accessed to build iteration domains, access relations and the identity schedule while, obviously, preserving the legality of the reconstruction in a cost-effective fashion. Our results demonstrate the high-quality of the lifting process, the coverage, and the potential impact on large quantum circuits. The next logical step is to customize the reconstruction process considering topological knowledge, qubit physical parameters and tailoring affine transformations to exploit domain knowledge.

References

[1] Frank Arute, Kunal Arya, Ryan Babbush, Dave Bacon, Joseph C Bardin, Rami Barends, Rupak Biswas, Sergio Boixo, Fernando GSL Brandao, David A Buell, et al. 2019. Quantum supremacy using a programmable superconducting processor. *Nature* 574, 7779 (2019), 505–510.

[2] Cedric Bastoul. 2004. Code generation in the polyhedral model is easier than you think. In *Proceedings. 13th International Conference on Parallel Architecture and Compilation Techniques, 2004. PACT 2004.* 7–16. https://doi.org/10.1109/PACT.2004.1342537

[3] Debjyoti Bhattacharjee, Abdullah Ash Saki, Mahabubul Alam, Anupam Chattopadhyay, and Swaroop Ghosh. 2019. MUQUT: Multi-Constraint Quantum Circuit Mapping on Noisy Intermediate-Scale Quantum Computers. arXiv:1911.08559 [quant-ph]

[4] Benjamin Bichsel, Maximilian Baader, Timon Gehr, and Martin Vechev. 2020. Silq: A High-Level Quantum Language with Safe Uncomputation and Intuitive Semantics. In *Proceedings of the 41st ACM SIGPLAN Conference on Programming Language Design and Implementation* (London, UK) *(PLDI 2020)*. Association for Computing Machinery, New York, NY, USA, 286–300. https://doi.org/10.1145/3385412.3386007

[5] Uday Bondhugula, Albert Hartono, J. Ramanujam, and P. Sadayappan. 2008. A Practical Automatic Polyhedral Parallelizer and Locality Optimizer. In *Proceedings of the 29th ACM SIGPLAN Conference on Programming Language Design and Implementation* (Tucson, AZ, USA) *(PLDI '08)*. ACM, New York,

NY, USA, 101–113. https://doi.org/10.1145/1375581.1375595

[6] Chun Chen, Jacqueline Chame, and Mary Hall. 2005. Combining Models and Guided Empirical Search to Optimize for Multiple Levels of the Memory Hierarchy. In *Proceedings of the International Symposium on Code Generation and Optimization (CGO '05)*. IEEE Computer Society, Washington, DC, USA, 111–122. https://doi.org/10.1109/CGO.2005.10

[7] Andrew M Childs, Eddie Schoute, and Cem M Unsal. 2019. Circuit transformations for quantum architectures. *arXiv preprint arXiv:1902.09102* (2019).

[8] Patrick J. Coles, Stephan J. Eidenbenz, Scott Pakin, Adetokunbo Adedoyin, John Ambrosiano, Petr M. Anisimov, William Casper, Gopinath Chennupati, Carleton Coffrin, Hristo N. Djidjev, David Gunter, Satish Karra, Nathan Lemons, Shizeng Lin, Andrey Y. Lokhov, Alexander Malyzhenkov, David Dennis Lee Mascarenas, Susan M. Mniszewski, Balu Nadiga, Dan O'Malley, Diane Oyen, Lakshman Prasad, Randy Roberts, Philip Romero, Nandakishore Santhi, Nikolai Sinitsyn, Pieter Swart, Marc Vuffray, Jim Wendelberger, Boram Yoon, Richard J. Zamora, and Wei Zhu. 2018. Quantum Algorithm Implementations for Beginners. *CoRR* abs/1804.03719 (2018). arXiv:1804.03719 http://arxiv.org/abs/1804.03719

[9] Luigi P Cordella, Pasquale Foggia, Carlo Sansone, and Mario Vento. 2004. A (sub) graph isomorphism algorithm for matching large graphs. *IEEE transactions on pattern analysis and machine intelligence* 26, 10 (2004), 1367–1372.

[10] Alexander Cowtan, Silas Dilkes, Ross Duncan, Alexandre Krajenbrink, Will Simmons, and Seyon Sivarajah. 2019. On the Qubit Routing Problem. In *14th Conference on the Theory of Quantum Computation, Communication and Cryptography (TQC 2019) (Leibniz International Proceedings in Informatics (LIPIcs), Vol. 135)*, Wim van Dam and Laura Mancinska (Eds.). Schloss Dagstuhl–Leibniz-Zentrum fuer Informatik, Dagstuhl, Germany, 5:1–5:32. https://doi.org/10.4230/LIPIcs.TQC.2019.5

[11] Andrew W Cross, Lev S Bishop, John A Smolin, and Jay M Gambetta. 2017. Open quantum assembly language. *arXiv preprint arXiv:1707.03429* (2017).

[12] Edward Farhi and Aram W Harrow. 2016. Quantum supremacy through the quantum approximate optimization algorithm. *arXiv preprint arXiv:1602.07674* (2016).

[13] Paul Feautrier. 1991. Dataflow analysis of array and scalar references. *International Journal of Parallel Programming* 20, 1 (01 Feb 1991), 23–53. https://doi.org/10.1007/BF01407931

[14] Sylvain Girbal, Nicolas Vasilache, Cédric Bastoul, Albert Cohen, David Parello, Marc Sigler, and Olivier Temam. 2006. Semi-automatic composition of loop transformations for deep parallelism and memory hierarchies. *International Journal of Parallel Programming* 34, 3 (2006), 261–317.

[15] Alexander S. Green, Peter LeFanu Lumsdaine, Neil J. Ross, Peter Selinger, and Benoît Valiron. 2013. Quipper: A Scalable Quantum Programming Language. In *Proceedings of the 34th ACM SIGPLAN Conference on Programming Language Design and Implementation* (Seattle, Washington, USA) *(PLDI '13)*. ACM, New York, NY, USA, 333–342. https://doi.org/10.1145/2491956.2462177

[16] Martin Griebl, Paul Feautrier, and Christian Lengauer. 2000. Index Set Splitting. *Int. J. Parallel Program.* 28, 6 (2000), 607–631. https://doi.org/10.1023/A:1007516818651

[17] Tobias Grosser, Armin Groesslinger, and Christian Lengauer. 2012. Polly—performing polyhedral optimizations on a low-level intermediate representation. *Parallel Processing Letters* 22, 04 (2012), 1250010.

[18] Jingzhe Guo and Mingsheng Ying. 2020. Software Pipelining for Quantum Loop Programs. *arXiv preprint arXiv:2012.12700* (2020).

[19] Aric Hagberg, Pieter Swart, and Daniel S Chult. 2008. *Exploring network structure, dynamics, and function using NetworkX*. Technical Report. Los Alamos National Lab.(LANL), Los Alamos, NM (United States).

[20] P. E. Hart, N. J. Nilsson, and B. Raphael. 1968. A Formal Basis for the Heuristic Determination of Minimum Cost Paths. *IEEE Transactions on Systems Science and Cybernetics* 4, 2 (1968), 100–107.

[21] Jeff Heckey, Shruti Patil, Ali JavadiAbhari, Adam Holmes, Daniel Kudrow, Kenneth R Brown, Diana Franklin, Frederic T Chong, and Margaret Martonosi. 2015. Compiler management of communication and parallelism for quantum computation. *ACM SIGARCH Computer Architecture News* 43, 1 (2015), 445–456.

[22] Justin Holewinski, Ragavendar Ramamurthi, Mahesh Ravishankar, Naznin Fauzia, Louis-Noël Pouchet, Atanas Rountev, and P. Sadayappan. 2012. Dynamic Trace-based Analysis of Vectorization Potential of Applications. In *Proceedings of the 33rd ACM SIGPLAN Conference on Programming Language Design and Implementation* (Beijing, China) *(PLDI '12)*. ACM, New York, NY, USA, 371–382. https://doi.org/10.1145/2254064.2254108

[23] IBM. 2018. Qiskit. https://qiskit.org

[24] IBM. 2021. IBM Quantum Services. https://quantum-computing.ibm.com/services

[25] Johannes Kepler University Linz Institute for Integrated Circuits. 2019. *IIC JKU - IBMQX QASM Circuits*. https://github.com/iic-jku/ibm_qx_mapping/tree/master/examples Online; accessed on August 2021.

[26] F. Irigoin and R. Triolet. 1988. Supernode Partitioning. In *Proceedings of the 15th ACM SIGPLAN-SIGACT Symposium on Principles of Programming Languages* (San Diego, California, USA) *(POPL '88)*. ACM, New York, NY, USA, 319–329. https://doi.org/10.1145/73560.73588

[27] Raban Iten, Romain Moyard, Tony Metger, David Sutter, and Stefan Woerner. 2020. Exact and practical pattern matching for quantum circuit optimization. arXiv:1909.05270 [quant-ph]

[28] Ali JavadiAbhari, Arvin Faruque, Mohammad J Dousti, Lukas Svec, Oana Catu, Amlan Chakrabati, Chen-Fu Chiang, Seth Vanderwilt, John Black, and Fred Chong. 2012. *Scaffold: Quantum programming language*. Technical Report. PRINCETON UNIV NJ DEPT OF COMPUTER SCIENCE.

[29] Ali JavadiAbhari, Shruti Patil, Daniel Kudrow, Jeff Heckey, Alexey Lvov, Frederic T Chong, and Margaret Martonosi. 2014. ScaffCC: a framework for compilation and analysis of quantum computing programs. In *Proceedings of the 11th ACM Conference on Computing Frontiers*. ACM, 1.

[30] Gushu Li, Yufei Ding, and Yuan Xie. 2019. Tackling the Qubit Mapping Problem for NISQ-Era Quantum Devices. In *Proceedings of the Twenty-Fourth International Conference on Architectural Support for Programming Languages and Operating Systems* (Providence, RI, USA) *(ASPLOS '19)*. ACM, New York, NY, USA, 1001–1014. https://doi.org/10.1145/3297858.3304023

[31] Dmitri Maslov, Sean M. Falconer, and Michele Mosca. 2008. Quantum Circuit Placement. *IEEE Transactions on Computer-Aided Design of Integrated Circuits and Systems* 27, 4 (2008), 752–763. https://doi.org/10.1109/TCAD.2008.917562

[32] Jarrod R McClean, Ian D Kivlichan, Damian S Steiger, Yudong Cao, E Schuyler Fried, Craig Gidney, Thomas Häner, Vojtěch Havlíček, Zhang Jiang, Matthew Neeley, et al. 2017. OpenFermion: The Electronic Structure Package for Quantum Computers. *arXiv preprint arXiv:1710.07629* (2017).

[33] Prakash Murali, Jonathan M. Baker, Ali Javadi-Abhari, Frederic T. Chong, and Margaret Martonosi. 2019. Noise-Adaptive Compiler Mappings for Noisy Intermediate-Scale Quantum Computers. In *Proceedings of the Twenty-Fourth International Conference on Architectural Support for Programming Languages and Operating Systems* (Providence, RI, USA) *(ASPLOS '19)*. ACM, New York, NY, USA, 1015–1029. https://doi.org/10.1145/3297858.3304075

[34] Jennifer Paykin, Robert Rand, and Steve Zdancewic. 2017. QWIRE: A Core Language for Quantum Circuits. In *Proceedings of the 44th ACM SIGPLAN Symposium on Principles of Programming Languages* (Paris, France) *(POPL 2017)*. ACM, New York, NY, USA, 846–858. https://doi.org/10.1145/3009837.3009894

[35] John Preskill. 2018. Quantum computing in the NISQ era and beyond. *Quantum* 2 (2018), 79.

[36] Revlib. 2021. *Revlib: An Online Resource for Reversible Functions and Circuits*. http://www.revlib.org/functions.php Online; accessed on August 2021.

[37] Yunong Shi, Nelson Leung, Pranav Gokhale, Zane Rossi, David I Schuster, Henry Hoffmann, and Frederic T Chong. 2019. Optimized compilation of aggregated instructions for realistic quantum computers. In *Proceedings of the Twenty-Fourth International Conference on Architectural Support for Programming Languages and Operating Systems*. 1031–1044.

[38] Marcos Yukio Siraichi, Vinícius Fernandes dos Santos, Caroline Collange, and Fernando Magno Quintão Pereira. 2019. Qubit Allocation As a Combination of Subgraph Isomorphism and Token Swapping. *Proc. ACM Program. Lang.* 3, OOPSLA, Article 120 (Oct. 2019), 29 pages. https://doi.org/10.1145/3360546

[39] Marcos Yukio Siraichi, Vinícius Fernandes dos Santos, Sylvain Collange, and Fernando Magno Quintao Pereira. 2018. Qubit Allocation. In *Proceedings of the 2018 International Symposium on Code Generation and Optimization* (Vienna, Austria) *(CGO 2018)*. ACM, New York, NY, USA, 113–125. https://doi.org/10.1145/3168822

[40] Seyon Sivarajah, Silas Dilkes, Alexander Cowtan, Will Simmons, Alec Edgington, and Ross Duncan. 2020. tket: a retargetable compiler for NISQ devices. *Quantum Science and Technology* 6, 1 (Nov 2020), 014003. https://doi.org/10.1088/2058-9565/ab8e92

[41] Bochen Tan and Jason Cong. 2020. Optimal Layout Synthesis for Quantum Computing. In *Proceedings of the 39th International Conference on Computer-Aided Design* (Virtual Event, USA) *(ICCAD '20)*. Association for Computing Machinery, New York, NY, USA, Article 137, 9 pages. https://doi.org/10.1145/3400302.3415620

[42] Bochen Tan and Jason Cong. 2020. Optimality Study of Existing Quantum Computing Layout Synthesis Tools. *IEEE Trans. Comput.* (2020), 1–12. https://doi.org/10.1109/TC.2020.3009140

[43] Swamit S Tannu and Moinuddin Qureshi. 2019. Ensemble of diverse mappings: Improving reliability of quantum computers by orchestrating dissimilar mistakes. In *Proceedings of the 52nd Annual IEEE/ACM International Symposium on Microarchitecture*. 253–265.

[44] Swamit S Tannu and Moinuddin K Qureshi. 2019. Not all qubits are created equal: a case for variability-aware policies for NISQ-era quantum computers. In *Proceedings of the Twenty-Fourth International Conference on Architectural Support for Programming Languages and Operating Systems*. 987–999.

[45] Nicolas Vasilache, Oleksandr Zinenko, Theodoros Theodoridis, Priya Goyal, Zachary DeVito, William S Moses, Sven Verdoolaege, Andrew Adams, and Albert Cohen. 2018. Tensor comprehensions: Framework-agnostic high-performance machine learning abstractions. *arXiv preprint arXiv:1802.04730* (2018).

[46] Anand Venkat, Mary Hall, and Michelle Strout. 2015. Loop and Data Transformations for Sparse Matrix Code. In *Proceedings of the 36th ACM SIGPLAN Conference on Programming Language Design and Implementation* (Portland, OR, USA) *(PLDI '15)*. ACM, New York, NY, USA, 521–532. https://doi.org/10.1145/2737924.2738003

[47] Sven Verdoolaege. 2010. isl: An Integer Set Library for the Polyhedral Model.. In *ICMS*, Vol. 6327. Springer, 299–302.

[48] Sven Verdoolaege, Juan Carlos Juega, Albert Cohen, José Ignacio Gómez, Christian Tenllado, and Francky Catthoor. 2013. Polyhedral Parallel Code Generation for CUDA. *ACM Trans. Archit. Code Optim.* 9, 4, Article 54 (Jan. 2013), 23 pages. https://doi.org/10.1145/2400682.2400713

[49] Sven Verdoolaege and Tobias Grosser. 2012. Polyhedral extraction tool. In *Second International Workshop on Polyhedral Compilation Techniques (IMPACT'12), Paris, France*, Vol. 141.

[50] R. Wille, D. Große, L. Teuber, G. W. Dueck, and R. Drechsler. 2008. RevLib: An Online Resource for Reversible Functions and Reversible Circuits. In *Int'l Symp. on Multi-Valued Logic*. 220–225. RevLib is available at http://www.revlib.org.

[51] Xin-Chuan Wu, Marc Grau Davis, Frederic T Chong, and Costin Iancu. 2020. QGo: Scalable Quantum Circuit Optimization Using Automated Synthesis. *arXiv preprint arXiv:2012.09835* (2020).

[52] Xiangzhen Zhou, Sanjiang Li, and Yuan Feng. 2020. Quantum circuit transformation based on simulated annealing and heuristic search. *IEEE Transactions on Computer-Aided Design of Integrated Circuits and Systems* 39, 12 (2020), 4683–4694.

[53] Alwin Zulehner, Alexandru Paler, and Robert Wille. 2018. Efficient mapping of quantum circuits to the IBM QX architectures. In *2018 Design, Automation Test in Europe Conference Exhibition (DATE)*. 1135–1138. https://doi.org/10.23919/DATE.2018.8342181